ACS Partner Journal

Journal of the American Society for Mass Spectrometry

pubs.acs.org/jasms

Research Article

Evaluating the Effects of Metal Adduction and Charge Isomerism on Ion-Mobility Measurements using *m*-Xylene Macrocycles as Models

Damilola S. Oluwatoba, Md Faizul Islam, Bozumeh Som, Ammon J. Sindt, Mark D. Smith, Linda S. Shimizu, and Thanh D. Do*

Cite This: *J. Am. Soc. Mass Spectrom.* 2022, 33, 840−850

Read Online

ACCESS | Metrics & More | Article Recommendations | Supporting Information

ABSTRACT: Gas-phase ion-mobility spectrometry provides a unique platform to study the effect of mobile charge(s) or charge location on collisional cross section and ion separation. Here, we evaluate the effects of cation/anion adduction in a series of xylene and pyridyl macrocycles that contain ureas and thioureas. We explore how zinc binding led to unexpected deprotonation of the thiourea macrocyclic host in positive polarity ionization and subsequently how charge isomerism due to cation (zinc metal) and anion (chloride counterion) adduction or proton competition among acceptors can affect the measured collisional cross sections in helium and nitrogen buffer gases. Our approach uses synthetic chemistry to design macrocycle targets and a combination of ion-mobility spectrometry mass spectrometry experiments and quantum mechanics calculations to characterize their structural properties. We demonstrate that charge isomerism significantly improves ion-mobility resolution and allows for determination of the metal binding mechanism in metal−inclusion macrocyclic complexes. Additionally, charge isomers can be populated in molecules where individual protons are shared between acceptors. In these cases, interactions via drift gas collisions magnify the conformational differences. Finally, for the macrocyclic systems we report here, charge isomers are observed in both helium and nitrogen drift gases with similar resolution. The separation factor does not simply increase with increasing drift gas polarizability. Our study sheds light on important properties of charge isomerism and offers strategies to take advantage of this phenomenon in analytical separations.

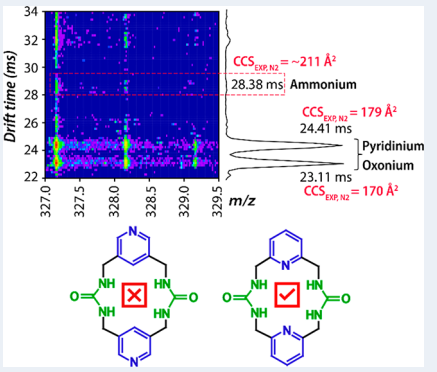

KEYWORDS: *ion-mobility mass spectrometry, charge isomerism, drift gas, metal adduction, collisional cross section*

INTRODUCTION

Advances in gas-phase techniques have had a profound impact on chemistry and biology.[1−7] The versatility of ionization methods has brought a wide range of molecules into vacuum for molecular identification and structural elucidation. The latter task often requires a high degree of structural fidelity between gas-phase ions and (often neutral) target species in their native condition. Ionization processes may preserve some and transform other noncovalent interactions, resulting in species with characteristics of both the gas-phase and the native condition (most often solution). Protonation, metal adduction, and charge isomerism are some of the key factors that determine these observations with mass spectrometry (MS).

Metal binding preionization and metal adduction (induced by ionization) have both been exploited in gas-phase separation of isomers. For example, Gaye et al.[8] used ion-mobility spectrometry mass spectrometry (IMS-MS) to separate a mixture of 16 monosaccharides consisting of 8 glucose diastereomers and their respective enantiomers. This clever approach measured collision cross sections (CCSs) of the complexes of the glucoses with either an amino acid (L-Ser) or dipeptide (L-Phe-Gly) or with both the dipeptide and a metal [Mn(II)]. Thus, each isomer was described by multiple CCS values of isomer:metal or isomer:peptide complexes. Similarly, Rister et al.[9] employed group I metal (Li^+, Na^+, K^+) adduction for steroid separation. Beyond metal adduction in the gas phase, several macrocycles (e.g., crown ethers,[10−14] valinomycin,[15] and cyclosporines[16]) function as ionophores in solution and have been investigated by MS. In some of these examples, metal complexes are formed via gas-phase chemistry while others are formed in solution and transferred into the gas phase via ionization or being a part of ion−ion/ion-neutral interactions in the gas phase.[17,18] Therefore, understanding the formation and selectivity of metal inclusion complexes in the gas phase and their native forms in solution is part of rigorous characterization efforts. Comparisons are often made between MS data and solution- or solid-phase data from nuclear

Received: February 1, 2022
Revised: April 9, 2022
Accepted: April 11, 2022
Published: April 26, 2022

https://doi.org/10.1021/jasms.2c00033
J. Am. Soc. Mass Spectrom. 2022, 33, 840−850

magnetic resonance (NMR)[16] or X-ray crystallography[19] or with spectroscopy coupled to the end of MS.[15]

Previously, we used small synthetic macrocycles to study the survivability and transformations of noncovalent interactions in the gas phase, including selective metal coordination and self-assembly. Macrocycles **1** and **2** (Figure 1A) are *m*-xylene

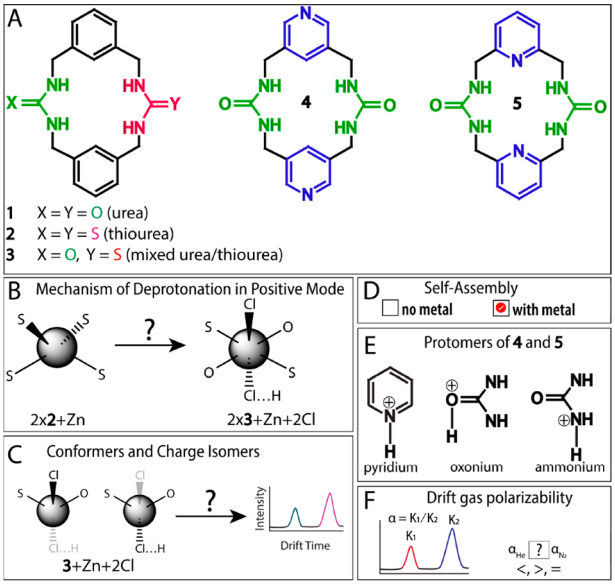

Figure 1. (A) 2D chemical structures of macrocycles **1**−**5**. The macrocycles are used as model structures to investigate (B) the mechanism of deprotonation in positive mode which may involve a transformation from a tetrahedral coordination (favored by **2**) into an octahedral coordination (by **3**). (C) Combined effect of charge and conformational isomerism, (D) effect of metals on self-assembly, and (E,F) effect of drift gas polarizability on separation factor of charge isomers.

macrocycles containing a pair of ureas or thioureas, respectively. Notably, **2** selectively recognizes and forms an inclusion complex with Zn^{2+} ($ZnCl_2$) composed of a noncovalent dimer of **2** stabilized by a Zn^{2+} center via Zn−S tetrahedral coordination.[20] However, the species observed in the MS data was $[2x(\mathbf{2})-H+Zn]^+$ (a singly charged, *deprotonated* dimer complex) and not $[2x(\mathbf{2})+Zn]^{2+}$ (a doubly charged dimer complex),[20] which was unexpected. The loss of a proton (deprotonation) occurred during the electrospray ionization (ESI) in positive mode.[20] We hypothesized that the counterion (Cl^-) participated in the initial complex formation and upon leaving abstracted a proton from the macrocyclic host. That process, if occurred, would have to be conformation-dependent. In this work, we designed and synthesized a new macrocycle (**3**) specifically to evaluate the model of proton abstraction by Cl^- anion and the roles of Zn^{2+} and Ca^{2+} cations in host−guest chemistry and self-assembly of macrocycles. The mixed urea/thiourea **3** also examines the competition between the two hydrogen bond directing groups on how the assembly could be stabilized by metals.

In addition to evaluating the mechanism of deprotonation in positive mode ESI, we also investigate charge isomerism in these macrocycles, i.e., the formation and preference of charge isomers, and the effect of charge isomerism on the measured CCSs. Charge isomers are often serendipitously discovered in IMS-MS experiments where the resolution of IMS-MS surpasses other analytical techniques for this type of molecule. Previous literature has used the term "protomers" to describe the molecular forms of the same species differed by the protonation sites. Notable examples include aniline,[21−24] benzocaine and its analogues,[23,25−34] nicotine,[35,36] and porphyrin derivatives.[21] The reported cases of charge isomerism have often been based on discrepancies observed in the arrival time distribution (ATD) obtained in polarized buffer gases of which *at least one feature has a CCS much larger than expected.* Taking benzocaine as an example, two features were observed in the ATD, and upon further investigation with ion-mobility selected IR spectroscopy and quantum mechanics (QM) modeling, they were assigned to be N-protonated (favored in solution) and O-protonated (favored in the gas phase).[37] However, charge isomerism has not been reported in metal-bound complexes. Here, we use the Zn-bound **3** complexes as the model system. Furthermore, the relative position of proton acceptors are examined with macrocycles **4** and **5**. The synthetic macrocycles **4** and **5** (Figure 1) are similar in size to **1**−**3** as they contain urea and/or thiourea hydrogen bonding motifs which can direct their assembly. These two macrocycles also display alternative coordination modes by employing the lone pairs of their pyridyl-N and urea-O as proton acceptors.

Here, we take a step toward controlling charge isomerism by considering "charges" in a broad context; i.e., charges can be from the metals and counterions adducted or bound to the host molecules or a proton being shared among multiple acceptors. Using a combination of organic synthesis, IMS-MS, IMS-MS/MS, and density functional theory (DFT) calculations, we show structure-dependent pathways that promote tautomerization in some macrocyclic models. Our work demonstrates that macrocycles and metal−macrocycle complexes are great models to assess the effect of charge preferences on the measured CCS. This will be a step closer to unravel the implication of charge isomerism in the mobilities of large biomolecules such as proteins where ions with higher charge states than the number of basic sites have routinely been observed.[38−40] Such findings will have a profound impact on our understanding of protein folding and unfolding in the gas phase.

MATERIALS AND METHODS

Macrocycle Synthesis and Characterization. The urea **1**,[41] thiourea **2**,[42] and pyridyl bisurea **5** *m*-xylene[43,44] macrocycles were synthesized as previously reported. The asymmetric macrocycle **3** was prepared such that it contains both urea and thiourea groups (see SI Scheme S1). Macrocycle **3** was crystallized by the vapor diffusion of H_2O into a dimethyl sulfoxide (DMSO) solution of **3** (20 mg/mL). Macrocycle **4**, the structural isomer of **5**, was synthesized starting from pyridine-3,5-dicarboxylic acid (Scheme S2), and crystals suitable for X-ray diffraction were obtained by heating macrocycle **4** in a 5 mL DMSO/acetonitrile (2:3 v/v) solution to 120 °C for 30 min, followed by slow cooling to room temperature at a rate of 1 °C/h. See the Supporting Information for characterization details. Other chemicals were used without further purification.

IMS-MS. For IMS-MS experiments, the stock samples were prepared at the concentration of 1 mg/1.1 mL of DMSO (2.7 mM). The stock was further diluted to the final concentration of 100 μM in pure LC-MS H_2O. Mass spectrometry and multifield ion-mobility spectrometry experiments were performed using an Agilent 6560 IMS-Q-TOF instrument

https://doi.org/10.1021/jasms.2c00033
J. Am. Soc. Mass Spectrom. 2022, 33, 840−850

(Agilent Technologies, Santa Clara, CA). The mass calibration and CCS were validated using the Agilent ESI-L tuning mix (diluted in 95:5 v/v ACN/H_2O). The ions were generated by ESI by a dual ESI/Agilent Jet stream source and a syringe pump at the rate of 30 μL/min. Instrument parameters were tuned based on the early work by Gabelica and co-workers.[45] The ions were stored in a source funnel and then pulsed into a 78.1 cm drift cell filled with a pressure at 3.94 Torr. The ions then traversed through the drift tube under the influence of a weak electric field and simultaneously collided with the stationary buffer gas. The size, shape, and net charge determined the velocity at which the ions drifted through the cell. Data were obtained in positive polarity over the course of 5.2 min with drift cell voltages of ΔV = 1490, 1390, 1290, 1190, and 1090 V in nitrogen and 900, 800, 700, 600, and 500 V in helium. For each species, the drift velocity is related to the reduced ion mobility, K_0, and used to calculate the momentum-transfer collision integral through the Mason-Schamp[15] equation, which is reported as the experimental CCS.

$$\mathrm{CCS} \approx \frac{3ze}{16N_0}\frac{1}{K_0}\sqrt{\frac{2\pi}{\mu k_B T}} \quad (1)$$

where e is the elementary charge, N is the gas number density of the drift gas, μ is the reduced mass of the ion and drift gas, K_B is the Boltzmann constant, and T is the drift-gas temperature. The ATDs and the mass spectra graphs were made using OriginPro. For all IM-MS experiments reported here, the same systems were characterized in both helium and nitrogen drift gases.

Distance Geometry (DG) Conformational Search. DG modeling was performed using the OpenEye OMEGA software[46] and the *macrocycle* module, the MMFF94s force field, and *dielectric_constant* set to 78.4 (water). The search successfully sampled all possible orientations of amines (*cis/cis*, *cis/trans*, *trans/trans*) and of the two benzyl rings (*syn/anti*). The theoretical CCS values of all conformers from the search were calculated using the trajectory method (TM) available in the Mobcal package[47,48] with the partial charges from QM. From this procedure, the CCS ranges and the largest possible CCS of **1** and **3** can be determined (see SI section S3). The model structures can be founded in the Supporting Information as compressed PDB files.

Quantum Mechanics Calculations. For [**3**+Zn+Cl]$^+$, the initial conformations were built using Avogadro version 1.2.0[49] starting from the reported structure of [**2**+Zn]$^{2+}$ (the bowl-like conformer where Zn^{2+} can maximize its interaction with S and O)[20] or the conformers where the amines are *cis/trans* (DG-generated) or *trans/trans* (X-ray structure; see SI section S6). The Cl^- ion was placed on top, inside, or below the macrocyclic host to evaluate its interaction with the aromatic benzyls and the amine protons. DFT calculations were geometrically optimized with Gaussian 16[50] at the B3LYP[51−54] level theory and Karlsruhe basis sets,[55] the Grimme's dispersion correction GD3,[56] and frequency calculation. Single-point energy values were reported. For [**4**+H]$^+$ and [**5**+H]$^+$, the X-ray crystal structures were used.

RESULTS AND DISCUSSION

Proton Abstraction of Chloride Anion Leads to Deprotonation in Positive Polarity. Our previous study[20] showed selective metal complexation of **2** and Zn^{2+} (from $ZnCl_2$). No Zn^{2+} complexes were observed with **1**. The dimeric [2x**2**−H+Zn]$^+$ complex consists of two off-axis "flat" **2** with four sulfurs equally "bonded" to a Zn center. Such offset is crucial for the sulfur coordination around Zn^{2+} to be in a distorted tetrahedral geometry (the sphalerite polymorph), with an average Zn−S distance of 2.5 Å. At low Zn^{2+} ($ZnCl_2$) concentrations, the dominant species was [2x**2**−H+Zn]$^+$, whereas increasing the concentration led to the presence of [**2**−H+Zn]$^+$. In both species, the observed macrocyclic host was *deprotonated*. A possible explanation is the thiol−thione tautomerization of thiourea promoted the deprotonation of NH as $S^-\cdots Zn^{2+}$ is a stronger interaction than $S\cdots Zn^{2+}$. We further hypothesized that the dimeric complex is formed stepwise starting with $ZnCl^+$ or $ZnCl_2$ initially making contact with one unit of **2**. As the Zn^{2+} tetrahedral coordination is satisfied by two units of **2**, the bond(s) between Zn^{2+} and Cl^- is weakened. Because the ionization polarity is positive, the dissociated Cl^- would be "protonated" by capturing a nearby hydrogen from the macrocyclic host. However, experiments with **2** never resulted in any complexes with Cl^-.

Here, we designed the macrocycle **3** with a mix of one thiourea and one urea. Given that the oxygen of urea does not form a stable interaction with Zn^{2+} (evident by macrocycle **1** showing no Zn^{2+} complexes[20]), the dimer of **3** cannot provide a strong tetrahedral coordination to stabilize the Zn^{2+} center as **2** does. As such, we may have a better chance to capture the intermediate complexes containing Cl^-.

Figure 2 shows two mass spectra of **3** with $ZnCl_2$ at 100:1 and 10:1 ratios (the latter has higher $ZnCl_2$ concentration). In addition to complexes containing Na^+ and K^+ (both are ubiquitous in MS solvents and easily picked up by MS), we observed [2x**3**+Zn+Cl]$^+$ but not its deprotonated form (i.e., [2x**3**−H+Zn]$^+$). This evidence supports our hypothesis that the Cl^- anion may be involved in the initial binding of Zn^{2+} to **3** (and **2**[20]) in solution. Additionally, we also observed species such as [2x**3**+Zn+2Cl+Na]$^+$ and [2x**3**+2Zn+3Cl]$^+$. It is important to note that the observed species could be related but not identical to those existing in solution. For example, the solution-phase species could be [2x**3**+Zn+2Cl] and [2x**3**+2Zn +4Cl]; both have a net charge of 0 and hence cannot be detected by MS. Nonetheless, the presence of Cl^--containing species suggests that the Zn center in the complex of **3** may

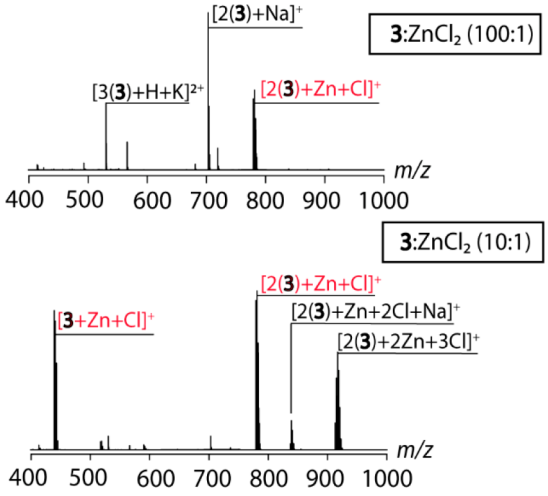

Figure 2. ESI-mass spectra of **3** with $ZnCl_2$ at 100:1 and 10:1 ratios. The concentration of **3** was kept constant at 100 μM.

https://doi.org/10.1021/jasms.2c00033
J. Am. Soc. Mass Spectrom. 2022, 33, 840−850

exist in an octahedral environment instead of a tetrahedral environment of Zn-bound **2** complexes. For the dimeric complex of **3** with Zn^{2+}, the metal center can be stabilized by two sulfurs, two oxygens, and two chlorides (see Figure 1B).

The dimeric complex is preferred over the monomeric complex $[3+Zn+Cl]^+$. The monomeric complex was only seen at a high $ZnCl_2$ ratio. The monomeric complex was likely the dissociated byproduct of the dimeric complex, or of a monomeric complex like [3+Zn+2Cl], which is neutral and thus cannot be detected by MS. The loss of a chloride anion to go from [3+Zn+2Cl] to $[3+Zn+Cl]^+$ can yield at least two geometric isomers distinguishable based on the distance between Cl^- and the NH proton (see Figure 1C).

Interestingly, a further inspection of the ATD of m/z 439, which corresponds to $[3+Zn+Cl]^+$, indicated that there were two distinct species, corresponding to two different modes of [Zn+Cl] binding to **3** (Figure 3A). We carefully checked to confirm that the second feature observed of m/z 439 in helium (or nitrogen) is not a post-IM product of a larger complex.

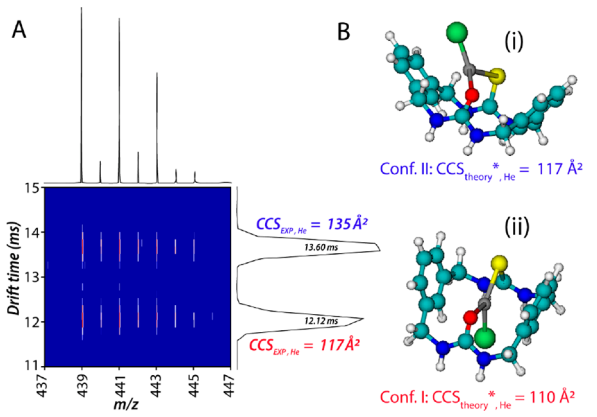

Figure 3. (A) Representative 2D plot of m/z vs drift time for $[3+Zn+Cl]^+$ (m/z 439). The isotope spacing is consistent with Zn and Cl containing species. (B) QM-optimized structures of two proposed models. Note that the reported theoretical CCS values (with the asterisk) are of the macrocyclic host and Zn+Cl modeled as two S atoms, thus they are expected to be smaller than the experimental values. The elements in the structures are color-coded; carbon (cyan), hydrogen (white), nitrogen (blue), oxygen (red), zinc (silver), and chloride (green).

Previous studies have suggested that anions (SO_4^{2-}/HSO_4^-, Cl^-, NO_3^-) could bind to the four urea hydrogens (NHs) of the *m*-xylene macrocycles, whereas cations such as metal cations (e.g., Zn^{2+}) would bind to the (soft) sulfurs of thioureas.[20,57,58] Therefore, two hypothetical binding motifs could be considered. The first motif (Figure 3B,i) would have $ZnCl^+$ (or $ZnCl_2$) as a single unit interacting mainly with thiourea-S. In this motif, the Cl^- anion(s) makes no contact with NHs, serves no role other than providing Zn coordination, and subsequently has no chance to abstract an NH proton. The second motif (Figure 3B,ii) has Zn^{2+} interacting with thiourea-S while the Cl^- anion (as a separate entity) interacts with NH protons. In this configuration, the Cl^- anion could easily capture a proton when the complex is energized. QM calculations on the optimized structures of these two models in the gas phase show configuration I is about 8 kcal/mol higher in energy than configuration II, which is consistent with the longer arrival time feature being more intense. Of note, while the macrocycle unit in both configurations adopts a "bowl"-like conformation, in configuration I, the binding of Cl^- to the amine hydrogens actually competes with the binding of Zn^{2+} to the urea-O/thiourea-S, making the macrocycle more compact and thus increasing ring strain.

Charge Isomerism Magnifies the Conformational Difference between the Two Charge Isomers of $[3+Zn+Cl]^+$. Given the two model structures from QM calculations (Figure 3B), the next logical step is to compare their theoretical CCS values to the experimental CCS values of the two features in Figure 3A. The gold standard for theoretical CCS calculation has been the TM available in the Mobcal package.[47,48] However, Mobcal does not have parameters for Zn^{2+} and Cl^- and works only with He as the buffer gas. Other software programs[59] may have generic parameters for Zn but are far less accurate at predicting CCS for small molecules than Mobcal TM.

The difference between the experimental value ($CCS_{He,EXP}$ = 117 Å^2) and the theoretical value from Mobcal TM ($CCS_{He*,Mobcal\ TM}$ = 110 Å^2; the asterisk denotes that the calculation was performed for with Zn and Cl modeled as two S) is small. Given the sizes (van der Waals radii), the buried Zn and Cl can contribute an additional of ~7 Å^2 to the total CCS_{He}. This is a reasonable assumption as we experimentally determined that counterions (Cl^-, NO_3^-, DMSO) contributed less than 10 Å^2 to the total CCS_{He} for macrocycles with similar size (see Supporting Information of ref 20).

Next, the longer arrival time feature has an experimental CCS value of 135 Å^2 in helium. The DG conformational search shows that the largest possible CCS of **3** is 120 Å^2 (see SI section S3 and Figure S1). Given that Zn+Cl can contribute ~7 Å^2, the predicted CCS_{He} is still much smaller than the experimental CCS_{He}. Essentially, Mobcal TM (or any existing CCS calculation software) is not accurate at predicting the CCS of this feature (configuration II). Our extensive conformational search eliminates the possibility that this large CCS corresponds to an extended conformer (SI section S3). Notably, consider the seminal case of benzocaine: the longer arrival time feature of the N protomer of benzocaine has an experimental CCS of 155 Å^2, and the reported theoretical CCS is only 144 Å^2 (the data were collected in N_2).[37] In other words, the relatively large differences between predicted and experimental CCS observed here and for benzocaine suggest that predicting CCS of the ions with longer arrival times requires more sophisticated treatments. The charge locations/distributions affect how the ions interact with the drift gas, which subsequently amplify any difference in structure between two tautomerization states of $[3+Zn+Cl]^+$.

Of note, one possibility that might lead to the presence of two ATD features in Figure 3A is the formation of an aquo-Zn complex (i.e., $[3+Zn+(H_2O)_n+Cl]^+$) that was dissociated into $[3+Zn+Cl]^+$ after exiting the drift cell. However, such a complex is unlikely to survive the heated drying gas (300 °C) at the source. Solvent clustering often leads to peak broadening[60] and not two well-resolved, baseline-separated peaks. Furthermore, as the dimer complex $[2x3+Zn+Cl]^+$ was observed before $[3+Zn+Cl]^+$ (at high $[ZnCl_2]$), if solvent clustering occurred, we should have observed more than only the feature in the ATD of the dimer (Figure S2). Finally, as shown in the latter section, we also observed two features in the ATD of $[3+Ca+Cl]^+$ (Figure S3), making it unlikely that both metals can populate the same kind of solvated complexes.

https://doi.org/10.1021/jasms.2c00033
J. Am. Soc. Mass Spectrom. 2022, 33, 840−850

Effect of Drift Gases. To address the role of drift gas, we collected the IMS-MS data of $[3+Zn+Cl]^+$ using nitrogen as the buffer gas. Nitrogen as IM gas would have more efficient declustering capabilities than helium. The ATDs show two well-resolved features similar to those in helium (see Figure 4).

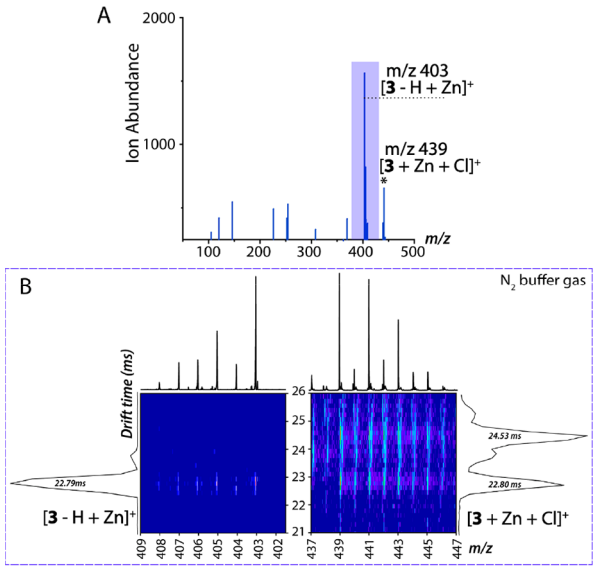

Figure 4. (A) Tandem IMS-MS/MS spectrum of $[3+Zn+Cl]^+$. (B) Representative ATDs of $[3\text{-}H+Zn]^+$ (m/z 403; left) and $[3+Zn+Cl]^+$ (m/z 439; right) at the same drift voltage. Data were collected in N_2.

To evaluate the effect of drift gases on the CCS differences between the isomers, we need to obtain their *theoretical* CCS values in N_2 and compare them with $CCS_{N2,EXP}$. We chose to convert the $CCS_{HE}{}^*{}_{,THEORY}$ values from Mobcal TM to $CCS_{N2}{}^*{}_{,THEORY}$ using the a linear approximation constructed by experimental CCS of 6 small molecules (m/z 250−609),[61] 5 Agilent tune-mix ions (m/z 322−1522),[61] and the macrocycles **1**, **2**, and **3**. The linear approximation is described by eq 2 (see also SI section S4 and Figure S4) for details. Note that eq 2 is only used to obtain $CCS_{N2,THEORY}$, whereas the reported CCS_{EXP} are absolute CCS.

$$CCS_{N2,THEORY} = CCS_{He,THEORY} \times 1.091 + 53.9 \quad (2)$$

Thus, the theoretical $CCS_{N2}{}^*{}_{,THEORY}$ values of configurations I and II are 174 and 182 Å^2, respectively, as seen in Table 1. It is important to note that our nitrogen results here are consistent with the helium data and the previous studies on gas-phase protomers where a larger discrepancy is observed for the features with longer drift times (the "solution-favored" protomer).[37] Also, similar to the report of benzocaine, here, the solution-phase isomer (configuration II; the charges are exposed) has a longer drift time than the gas-phase isomer (configuration I; the charges are buried).

Table 1. CCS_{EXP} and CCS_{THEORY} of $[3+Zn+Cl]^+$

drift gas	CCS_{EXP} (Å^2)	$CCS_{THEORY}{}^*$ (Å^2)
He	117	110
	135	117
N_2	186	174[a]
	200	182[a]

*Values were obtained by Mobcal TM with Zn and Cl modeled as S. [a]Values were converted from $CCS_{He,THEORY}$ using eq 2.

Warnke et al.[37] suggested that CCS calculation methods have not considered the charge effect in polarizable drift gases (N_2). Here, the separations of two species using He are significantly better than those in N_2 (see Table 1; $\Delta CCS_{N2,EXP}$ = 14 Å^2 vs $\Delta CCS_{He,EXP}$ = 18 Å^2; see also Table S3 for the calculated degrees of peak separation[61]), suggesting that gas polarizability may not be the sole factor.

Prior work on benzocaine protomers displayed poorer separation in helium than in nitrogen.[7,37] Our results show an opposite trend where the IM measurements in helium yield a similar if not better "resolution". In our case, the isomers are different in both conformations and charge locations. Apparently, the "charge" effect magnifies the conformational difference (from ∼7−8 to 14−18 Å^2). Although the net charge of both configuration is +1, the local partial charges that interact with the drift gas molecules are different. Because the effect of "charge" always outweighs the effect of size and shape, the effect of charge isomerism will be greater than the effect of conformational isomerism. In fact, McLean and co-workers[62] showed that the effects of drift gas polarizability vary with analyte classes and charge states. However, going from helium, argon, nitrogen, to carbon dioxide, ΔCCS between species of the same class and charge state (e.g., P-Ala6 and P-Ala13 or maltose and maltohexanose) remain relatively constant,[62] which could explain similar CCS differences between charge isomers of the *m*-xylene macrocycles in helium and nitrogen.

Finally, we performed the IMS-MS/MS experiments of the precursor ion m/z 439 ($[3+Zn+Cl]^+$) to further confirm the ATD assignments in Figure 3. Because we use an IMS-QTOF instrument and ion activation (collision-induced dissociation) is after the drift cell, the product ions have the drift time as its precursor ion.[20]

In Figure 4A, the main product ion is m/z 403, which corresponds to $[3\text{-}H+Zn]^+$. The isotopic spacing confirms that this is a Zn-containing species. The drift time of the m/z 403 product ion is the same as the shorter arrival time feature of m/z 439 (configuration I, Figure 4B). In order for $[3\text{-}H+Zn]^+$ to form, the to-be-dissociated Cl^- must be positioned near a H proton, and only in conformation I (Figure 3B,ii) is the proton abstraction from an amine possible. Thus, the data support our assignments. The data also support that the formation of $[2\text{-}H+Zn]^+$ and $[2x2\text{-}H+Zn]^{2+}$ reported in Link et al. are due to dissociated Cl^- abstracting an amine proton during positive mode ESI.

In summary, our data support the hypothesis that the binding of Zn^{2+} to *m*-xylene macrocycles containing thiourea (sulfur) involves the counterions. Furthermore, our study of **3** complexed with Zn^{2+} and Cl^- suggests that charge isomers can be formed by adducting the molecule with cations/anions in such a way that these mobile charged units can be rearranged in different configurations.

Furthermore, our data show that (a) the no or poor treatment of charge effect hinders the accuracy of CCS calculation methods for systems of charge isomers, and (b) unlike linear molecules like benzocaine,[7] the choices of drift gas (helium vs nitrogen) yield an opposite trend in terms of separation factor.

There can be multiple trends for different types of molecules, rather than one trend that fits all. The drift time is a function of CCS, reduced mass, and charge. Asbury and Hill[63] showed that the separation factor of chloroaniline and

https://doi.org/10.1021/jasms.2c00033
J. Am. Soc. Mass Spectrom. 2022, 33, 840−850

iodoaniline is better in helium than in nitrogen. As the drift gas polarizability increases (He < N_2; 0.205 × 10^{-24} cm^3 for He and 1.740 × 10^{-24} cm^3 for N_2),[64] the velocity of the chloroaniline ion decreases relative to the iodoaniline ion. Moreover, because the drift time is not a function of only the gas polarizability, the effect of reduced mass or charge could also be significant. In helium, the reduced mass is similar to the mass of He, whereas in highly polarizable gas such as CO_2 (polarizability of 2.911 × 10^{-24} cm^3 > N_2), the reduced mass will better reflect the mass of the analyte. Thus, in the case of chloro- versus iodoaniline, the separation factors are high for He and CO_2 buffer gases but poor in N_2.[63] To recap, increasing drift gas polarizability does not always lead to a better separation factor.

Ca^{2+} Stabilizes Oligomeric Structures of Macrocycles. In our previous study, some oligomers (clusters) of **1** and **2** were observed, albeit with low intensity.[20] Here, in an effort to demonstrate the unique binding of Zn^{2+} to thiourea containing *m*-xylene macrocycles, we discovered a unique behavior of Ca^{2+}. The presence of this metal cation increased the abundance of oligomers of **3** observed in the mass spectrum (Figure 4A). Notably, with Zn^{2+}, we did not observe any clusters larger than a dimer. However, with Ca^{2+} ($CaCl_2$), a range of large clusters of **3** were detected. The largest cluster was an octamer. At low Ca^{2+} ($CaCl_2$) concentration, the dominant species were doubly charged clusters of **3** with Ca^{2+} (no Cl^-). At high Ca^{2+}, complexes containing both Ca^{2+} and Cl^- were detected such as $[\mathbf{3}+Ca+Cl]^+$. IMS measurements also showed two distinct features, as seen in the case of Zn^{2+}. Figure S6 shows the ATDs of Ca^{2+}-adducted oligomers where multiple features corresponding to post-IM dissociated oligomers were observed. This phenomenon (loss of neutral species post IM for IM-QTOF instruments) has been discussed in detail.[65] The post-IM dissociation of oligomers of **3** indicates that the oligomeric structures are fragile in the gas phase.

The question is whether Ca^{2+} contributed to the formation of clusters or mainly served as a (charge) carrier to make the detection of these (neutral) clusters possible. The *m*-xylene urea macrocycle **1** self-assembled into a range of ordered structures via hydrogen bonding and π-stacking,[41] while the thiourea **2** assembles via edge-to-face slabs of the hydrogen bond network composed of 12 atom circuits with four different sulfurs in each circuit.[42] In a previous study, in the absence of added salt, only oligomers of **1** were detected,[20] indicating that the edge-to-face assembly is less stable than column assembly. From SI section S6, the assembly of **3** is similar to that of **2**. We argue that because the oxygens (urea) and sulfurs (thiourea) of **3** are part of an intricate hydrogen bond network, a protonation/deprotonation, which is required for the cluster to carry nonzero charge, would weaken the assembly. Such a problem can be overcome by forming adducts with a cation such as Ca^{2+}, as seen in our data. However, we did not observe the same effect with other metal cations such as Na^+, K^+, or Zn^{2+}, suggesting that Ca^{2+} could have another role in addition to being a charge carrier. We hypothesize that a binding of a single Ca^{2+} to one unit of **3** helps maintain the macrocyclic host conformation to stabilization of hydrogen bonding in the gas phase. The experimental CCS values of the calcium-adducted clusters are shown in (Figure 5B). The doubly charged species ($+Ca^{2+}$) have CCS values larger than those of the singly charged species ($+Ca^{2+}+Cl^-$), suggesting that these are two different assembly

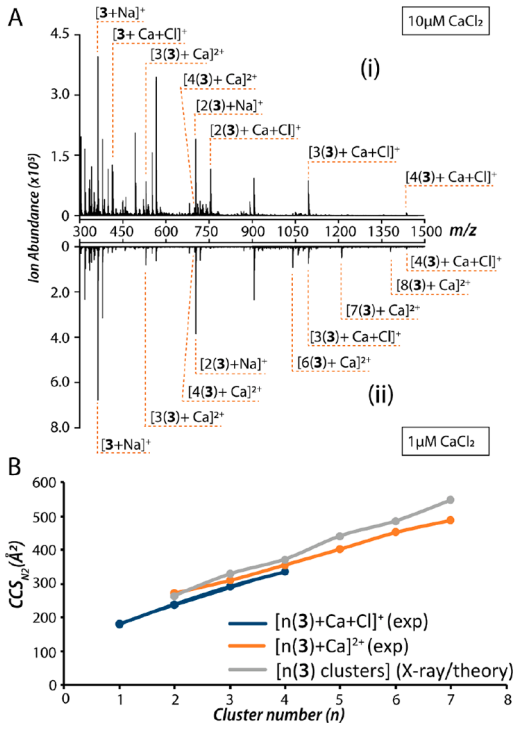

Figure 5. (A) Representative mass spectra of **3** with $CaCl_2$ at (i) 10 μM and (ii) 1 μM. (B) Experimental and theoretical CCSs of clusters of **3** in N_2.

modes. The experimental values are smaller than the theoretical CCSs, indicating that some structural rearrangements occurred in the gas phase.

***N*-Pyridyl Bisurea *m*-Xylenes: The Protomers.** In the first section, for **3**, the effect of charge isomerism was observed as a result of varying the positions of the cations (Zn^{2+}) and anions (Cl^-). There was no change in the protonation of the macrocyclic unit ($z = 0$). Here, we attempted to protonate the macrocycles and watch for protomers. The formation of protomers is often induced by a proton transfer among acceptor atoms,[24,25,30,32,66] but how easy for it to occur? Here, we evaluate whether having two proton acceptors is sufficient for protomer formation under standard MS ionization condition, or if any other factor may influence the process.

To do so, we studied two *m*-xylene macrocycle analogues where the benzyl rings were replaced with pyridine rings. The isomers **4** and **5** differ by the orientations of the pyridyl-N to the urea-O. Within these macrocycles, the two probable proton acceptors are the pyridyl-N ($pK_a \sim 6.6$ for the conjugate acid similar to 2,6-lutidine[67]) and the urea-carbonyl ($pK_a \sim -3.0$; conjugate acid). The pyridyl-N is a lot more ready to accept a proton than the carbonyl. In addition, the proximity between the pyridyl-N and ureas also influences their chemistry, as demonstrated by their assembly in the solid state. Newly synthesized macrocycle **4** forms columns are held together by a 3-centered urea−urea hydrogen bonding motif with hydrogen bond lengths of N1(H1)···O1 = 2.902(10) Å and N2(H2)···O1 = 2.847(11) Å. However, the proximity of pyridyl-N to the urea group in **5** affords columns in which the urea NHs interact with two different acceptors (see section S7).[43,44]

In the ATD of **4**, only one feature was observed in the drift time region (Figure 6, top left panel). In standard MS ionization with heated nebulizing and drying gases, a proton transfer via a solvent bridge cannot occur. In **4**, the pyridyl-N

https://doi.org/10.1021/jasms.2c00033
J. Am. Soc. Mass Spectrom. 2022, 33, 840−850

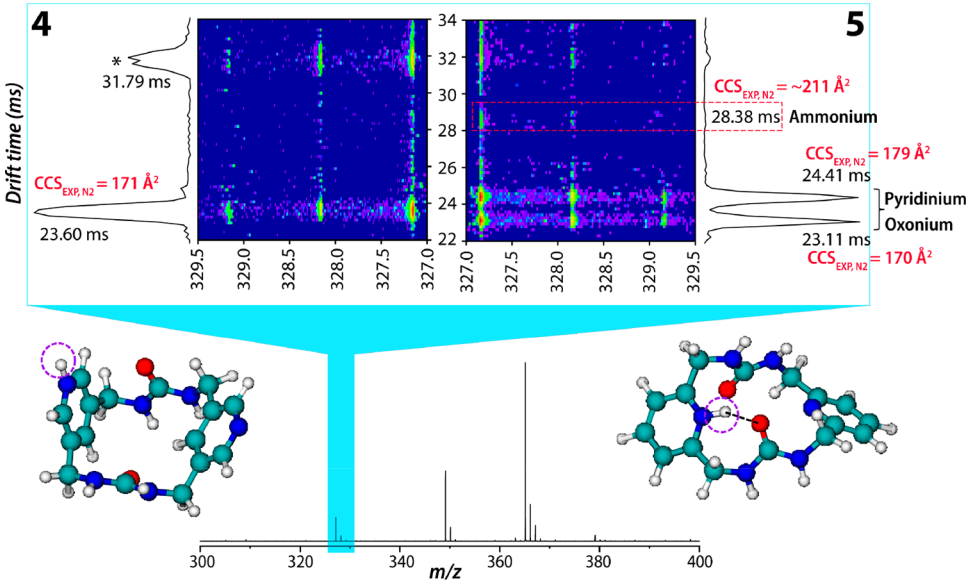

Figure 6. Representative 2D plot of protonated species of **4** and **5**. QM-optimized structures of $[4+H]^+$ and $[5+H]^+$. The latter shows a shared proton between pyridyl-N and urea-O. The feature annotated with an asterisk corresponds to a post-IM dissociated dimer.

does not share its proton with other acceptors. The energy difference between the geometry-optimized pyridyl-N protomer and the urea-O protomer is 15 kcal/mol. As the difference in energy of 1.4 kcal/mol results in a 10:1 ratio, without any perturbation to the system (e.g., a proton transfer pathway, a very high ionization voltage, etc.), the urea-O protomer of **4** should not be observed. Note that the feature at 32 ms corresponds to a post-IM dissociated product where a singly charged dimer successfully traversed the drift cell but was dissociated, lost a neutral monomer, and detected as a singly charged monomer. This event was discussed in detail in our previous work on similar systems.[20] Of note, the width of the ATD of **4** is greater than those of **5**, implying that there may be unresolved conformers that cannot be separated with our 78.1 cm drift tube.

On the other hand, in **5**, the ATD shows two distinct features. Of note, Shimizu and co-workers showed that protonation of **5** by naphthalene-1,5-disulfonic acid (H_2NDS) led to two salt cocrystal solvates in which the macrocyclic host adopted two distinct conformers: step-shaped with the urea groups in *trans*−*cis* configuration and bowl-shaped with the ureas in *trans*−*trans* configuration.[43] In fact, these "doubly protonated" species in the solid state are the closest references for the gas-phase structures obtained by MS. However, in the X-ray structures with H_2NDS,[43] both *N*-pyridyls were protonated (z = +2), whereas here, we detected only the singly charged species (z = +1).

The CCS difference between the step and bowl conformers of **5** is only 1 Å^2 (see Figure S7), and if this was the case, our IMS-MS should not have sufficient resolving power to distinguish them. In fact, previous studies of *m*-xylene macrocycles using IMS-MS were able to indirectly identify several conformers only when comparing the protonated/deprotonated species with the cation/anion adducted species.[20] It was not possible to resolve conformers of the isobaric species. Here, the CCS difference of the two observed species in N_2 is ~9 Å^2. Thus, we conclude that the effect of a shared protons between two acceptors contributed significantly to the difference in drift time (and CCS) we observed for the two conformers of **5**. On a side note, macrocycles are great systems to strategically design molecules with a shared proton. An interesting example is biliazarine by Zeigler and co-workers,[68] a phthalocyanine analogue where a hydrogen bond closes the ring.

In summary, the main difference between **4** and **5** is the close proximity of the pyridyl-N and urea-O in **5**, which allows for a proton transfer. The proton transfer between the two acceptors can account for the two features observed in the ATD of **5** (m/z 327) at 23 and 24 ms (Figure 6, top right panel). The pyridyl protonation and the urea−carbonyl protonation have essentially the same energy, consistent with the two features in the ATD having similar intensities. Of note, the 2D sketches may make it look like the pyridyl-N and urea-N were closer in space than between pyridyl-N and urea-O. However, protonation of urea-N is unlikely. For urea/thiourea alone, experimental and theoretical studies established that the oxygen/sulfur is more likely to pick up a proton (oxonium/sulfonium) than the nitrogen (ammonium).[69−71] Interestingly, there is a faint feature at 28 ms, which could possibly assigned to the urea-N protomer ($CCS_{N2,EXP}$ = 211 Å^2). This protomer is ~12 kcal/mol higher in energy than other two protomers, and its intensity reflects this difference. In addition, the same features (protomers) were observed when He was the drift gas (Figure S8). Therefore, similar to the charge isomers of **3**, the protomers of **5** can be observed in both N_2 and He with similar CCS differences (He is slightly better), indicating that the polarizability of the buffer gas may not be the main factor. Table 2 summarizes the experimental CCSs of the protomers

Table 2. CCS_{EXP} of $[5+H]^+$ and $[1+H]^+$ Protomers

		CCS_{EXP} (Å^2)	
macrocycle	protomer	N_2	He
5	pyridinium	179	115
	oxonium	**170**	**105**
	ammonium	211	
1	oxonium	**169**	**106**
	ammonium	188	137

https://doi.org/10.1021/jasms.2c00033
J. Am. Soc. Mass Spectrom. 2022, 33, 840−850

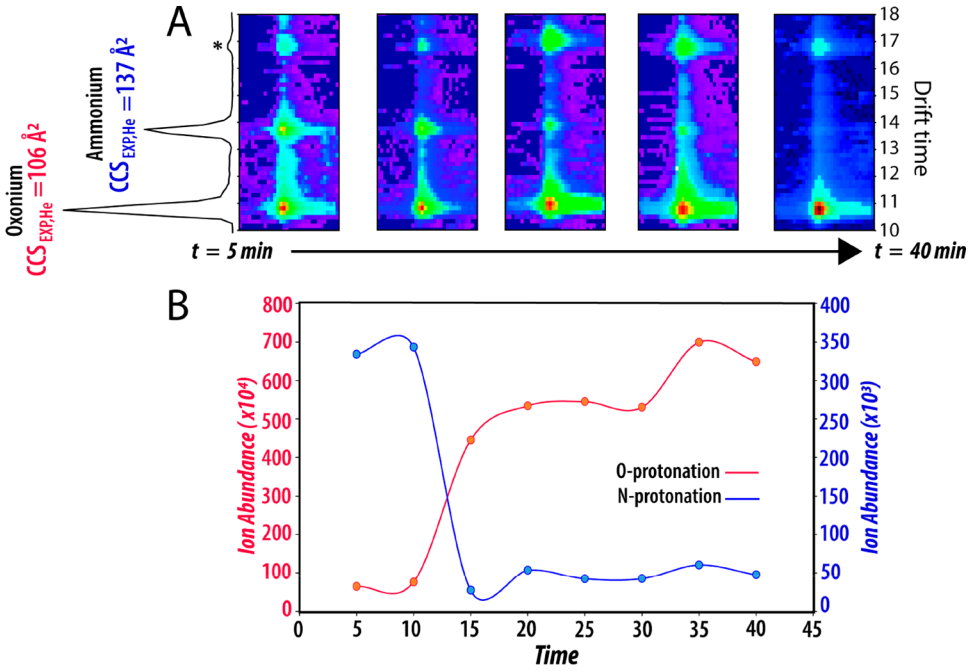

Figure 7. (A) Time evolution of the ATDs of $[\mathbf{1}+H]^+$ at m/z 325 going from a wet to a dry source chamber. Three ATD features were observed corresponding to the O-protonated, N-protonated, a dimer post IM-dissociated species. (B) Ion abundances of the two protomers. The drift gas is He. Post-IM dissociated dimer is labeled with an asterisk. Data were collected in He.

of $[\mathbf{5}+H]^+$. This appears to contradict earlier studies of protomers of linear molecules where the N and O protomers were observed in He but less resolved than the protomers detected in N_2.[7,37]

Recall the faint feature at 28.38 ms in Figure 6 that we tentatively assigned as the ammonium ion (the N protomer) of **5**. The abundance of this feature is low as the pyridinium (pyridyl-N protomer) and oxonium (carbonyl-O protomer) are strongly favored. Nonetheless, the N and O protomers could fairly compete when the pyridyl-N is removed, which is going back from **5** to the macrocycle **1**.

In nonstandard MS ionization conditions, the Attygalle group has further investigated conditions that promote tautomerization. Notably, moistened nitrogen gas stream at the source enhanced the detection of the N protomer of benzocaine.[24,25,30,32,66] Interestingly, we observed similar phenomenon when we revisited macrocycle **1** previously shown to have only one feature in the ATD of $[\mathbf{1}+H]^+$ ions. Our method to create a humidified source chamber is less sophisticated than that of the Attygale group,[24,25,30,32,66] as we simply wetted the source with water/methanol prior to data acquisition. Nonetheless, as the source becomes dry over time, Figure 7 shows the evolution of the $[\mathbf{1}+H]^+$'s ATD going from a humidified to a dry environment over a period of ~40 min. Helium buffer gas was used in this case. The shortest arrival time feature was assigned to be the urea O protomer ($CCS_{He,EXP}$ = 106 Å^2), the middle feature to be the urea N protomer ($CCS_{He,EXP}$ = 137 Å^2), and the longest arrival time feature to be the post-IM dimer. The intensity of the middle feature is gradually depleted over time as the humidity of the source chamber decreased. The water vapor may allow kinetic trapping of the solution-phase N protomer, whereas given enough time, the O protomer takes over. Similar data were obtained in nitrogen, and the CCS values are reported in Table 2.

SUMMARY AND CONCLUSIONS

Noncovalent interactions play a fundamental role in chemistry of life, from molecular recognition to protein folding and self-assembly. MS has become a powerful technique to study these interactions, but what occurs during and after the ionization may produce species with both characteristics of the native and gas-phase conditions. Here, we demonstrate that carefully designed macrocycles are excellent model systems to investigate metal adduction, self-assembly, and charge isomerism that are part of important noncovalent interactions.

Using an asymmetric urea/thiourea macrocycle (**3**), we validate the hypothesis that the deprotonation of metal-bound complexes observed in positive polarity involves a counterion (Cl^-) abstracting a proton upon leaving. We also demonstrate that protomers can be observed in two types of systems. The first type is composed of complexes containing charged adducts such as metals or counterions. Those cations/anions that cause structural (re)arrangement can lead to a small change in conformation, which is then further magnified by interaction with drift gases. The second type includes molecules in which a proton can be shared among multiple atoms with similar proton affinities or under a perturbation that favors charge transfer. However, while previous studies suggested that the drift gas determines the resolving power of the protomers,[7,27,37] our data show that N_2 and He have similar effect on the macrocyclic systems. Moreover, interactions of the protomers with drift gases amplify the conformational difference, suggesting that observation of protomers can be exploited to further enhance gas phase separation and identification of unknowns.

The model systems of charge isomers with accurate CCS measurements will provide experimental data for future refinement of CCS calculation methods. Finally, the detection of charge isomers in IMS-MS should be investigated in the context of systems such as peptides and small proteins, as they

https://doi.org/10.1021/jasms.2c00033
J. Am. Soc. Mass Spectrom. 2022, 33, 840−850

may introduce a novel approach to indirectly probe secondary structures and protein−protein interactions. For example, one can probe structures of a peptide/protein by using unnatural amino acids containing pyridines and rely on IMS and MS/MS data to identify the residues or backbone segments that interact with the unnatural amino acid.

■ ASSOCIATED CONTENT

Supporting Information

The Supporting Information is available free of charge at https://pubs.acs.org/doi/10.1021/jasms.2c00033.

Additional materials and methods, synthesis, NMR, and X-ray characterizations of the macrocycles, additional MS figures (PDF)

Distance geometry conformational sampling data for **3** (PDB)

Distance geometry conformational sampling data for **4** (PDB)

■ AUTHOR INFORMATION

Corresponding Author

Thanh D. Do − *Department of Chemistry, University of Tennessee, Knoxville, Tennessee 37996, United States*; Email: tdo5@utk.edu

Authors

Damilola S. Oluwatoba − *Department of Chemistry, University of Tennessee, Knoxville, Tennessee 37996, United States*; orcid.org/0000-0001-9791-9408

Md Faizul Islam − *Department of Chemistry and Biochemistry, University of South Carolina, Columbia, South Carolina 29208, United States*

Bozumeh Som − *Department of Chemistry and Biochemistry, University of South Carolina, Columbia, South Carolina 29208, United States; Department of Chemistry, University of Ghana, Legon, Accra, Ghana*

Ammon J. Sindt − *Department of Chemistry and Biochemistry, University of South Carolina, Columbia, South Carolina 29208, United States*

Mark D. Smith − *Department of Chemistry and Biochemistry, University of South Carolina, Columbia, South Carolina 29208, United States*

Linda S. Shimizu − *Department of Chemistry and Biochemistry, University of South Carolina, Columbia, South Carolina 29208, United States*

Complete contact information is available at: https://pubs.acs.org/10.1021/jasms.2c00033

Author Contributions

T.D.D. conceived the project. D.S.O. and T.D.D. collected the IMS-MS data and performed QM calculations. F.I., B.S., and A.J.S. synthesized the macrocycles **3** and **4**. M.D.S. performed the X-ray crystallography characterizations. L.S.S. led the synthesis team. D.S.O. wrote the first draft of the manuscript, and all authors contributed to its revision.

Funding

The synthesis and self-assembly work was supported in part by the National Science Foundation CHE-1904386.

Notes

The authors declare no competing financial interest.

■ ACKNOWLEDGMENTS

We gratefully acknowledge the laboratory start-up research support from the University of Tennessee and Department of Chemistry and the Global Academic Support Program from Agilent.

■ REFERENCES

(1) Zheng, X.; Wojcik, R.; Zhang, X.; Ibrahim, Y. M.; Burnum-Johnson, K. E.; Orton, D. J.; Monroe, M. E.; Moore, R. J.; Smith, R. D.; Baker, E. S. Coupling Front-End Separations, Ion Mobility Spectrometry, and Mass Spectrometry For Enhanced Multidimensional Biological and Environmental Analyses. *Annu. Rev. Anal. Chem.* **2017**, *10* (1), 71−92.

(2) Zhang, X.; Quinn, K.; Cruickshank-Quinn, C.; Reisdorph, R.; Reisdorph, N. The application of ion mobility mass spectrometry to metabolomics. *Curr. Opin. Chem. Biol.* **2018**, *42*, 60−66.

(3) Stuchfield, D.; Barran, P. Unique insights to intrinsically disordered proteins provided by ion mobility mass spectrometry. *Curr. Opin. Chem. Biol.* **2018**, *42*, 177−185.

(4) Lanucara, F.; Holman, S. W.; Gray, C. J.; Eyers, C. E. The power of ion mobility-mass spectrometry for structural characterization and the study of conformational dynamics. *Nat. Chem.* **2014**, *6* (4), 281−294.

(5) Hinz, C.; Liggi, S.; Griffin, J. L. The potential of Ion Mobility Mass Spectrometry for high-throughput and high-resolution lipidomics. *Curr. Opin. Chem. Biol.* **2018**, *42*, 42−50.

(6) Chouinard, C. D.; Wei, M. S.; Beekman, C. R.; Kemperman, R. H.; Yost, R. A. Ion Mobility in Clinical Analysis: Current Progress and Future Perspectives. *Clin. Chem.* **2016**, *62* (1), 124−33.

(7) Gabelica, V.; Marklund, E. Fundamentals of ion mobility spectrometry. *Curr. Opin. Chem. Biol.* **2018**, *42*, 51−59.

(8) Gaye, M. M.; Nagy, G.; Clemmer, D. E.; Pohl, N. L. Multidimensional Analysis of 16 Glucose Isomers by Ion Mobility Spectrometry. *Anal. Chem.* **2016**, *88* (4), 2335−2344.

(9) Rister, A. L.; Martin, T. L.; Dodds, E. D. Application of Group I Metal Adduction to the Separation of Steroids by Traveling Wave Ion Mobility Spectrometry. *J. Am. Soc. Mass Spectrom.* **2019**, *30* (2), 248−255.

(10) Williams, S. M.; Brodbelt, J. S.; Huang, Z. L.; Lai, H. G.; Marchand, A. P. Complexation of silver and co-recovered metals with novel aza-crown ether macrocycles by electrospray ionization mass spectrometry. *Analyst* **2003**, *128* (11), 1352−1359.

(11) Kimura, K.; Sakamoto, H.; Kado, S.; Arakawa, R.; Yokoyama, M. Studies on metal-ion complex formation of crown ether derivatives incorporating a photoionizable spirobenzopyran moiety by electrospray ionization mass spectrometry. *Analyst* **2000**, *125* (6), 1091−1095.

(12) Sherman, C. L.; Brodbelt, J. S.; Marchand, A. P.; Poola, B. Electrospray ionization mass spectrometric detection of self-assembly of a crown ether complex directed by pi-stacking interactions. *J. Am. Soc. Mass Spectrom.* **2005**, *16* (7), 1162−1171.

(13) Kellner, I. D.; von Gernler, M. S.; Tzirakis, M. D.; Orfanopoulos, M.; Drewello, T. The Influence of Alkali Metal Cation Size on the Formation and Dissociation of Crown Ether Fullerene Dimers in Electrospray Mass Spectrometry. *J. Phys. Chem. C* **2016**, *120* (1), 786−792.

(14) Shou, W. Z.; Browner, R. F. Evaluation of crown ether complexation for elemental electrospray mass spectrometry. *Anal. Chem.* **1999**, *71* (16), 3365−3373.

(15) Sato, E.; Hirata, K.; Lisy, J. M.; Ishiuchi, S. I.; Fujii, M. Rethinking Ion Transport by Ionophores: Experimental and Computational Investigation of Single Water Hydration in Valinomycin-K(+) Complexes. *J. Phys. Chem. Lett.* **2021**, *12* (6), 1754−1758.

(16) Gray, A. L. H.; Steren, C. A.; Haynes, I. W.; Bermejo, G. A.; Favretto, F.; Zweckstetter, M.; Do, T. D. Structural Flexibility of Cyclosporine A is Mediated by Amide Cis-Trans Isomerization and

the Chameleonic Roles of Calcium. *J. Phys. Chem. B* **2021**, *125* (5), 1378−1391.
(17) McLuckey, S. A.; Huang, T. Y. Ion/ion reactions: new chemistry for analytical MS. *Anal. Chem.* **2009**, *81* (21), 8669−8676.
(18) Coon, J. J.; Ueberheide, B.; Syka, J. E. P.; Dryhurst, D. D.; Ausio, J.; Shabanowitz, J.; Hunt, D. F. Protein identification using sequential ion/ion reactions and tandem mass spectrometry. *Proc. Natl. Acad. Sci. U.S.A.* **2005**, *102* (27), 9463−9468.
(19) Brocker, E. R.; Anderson, S. E.; Northrop, B. H.; Stang, P. J.; Bowers, M. T. Structures of Metallosupramolecular Coordination Assemblies Can Be Obtained by Ion Mobility Spectrometry−Mass Spectrometry. *J. Am. Chem. Soc.* **2010**, *132*, 13486−13494.
(20) Link, B. A.; Sindt, A. J.; Shimizu, L. S.; Do, T. D. Selective host-guest chemistry, self-assembly and conformational preferences of m-xylene macrocycles probed by ion-mobility spectrometry mass spectrometry. *Phys. Chem. Chem. Phys.* **2020**, *22* (17), 9290−9300.
(21) Lalli, P. M.; Iglesias, B. A.; Toma, H. E.; Sa, G. F.; Daroda, R. J.; Silva Filho, J. C.; Szulejko, J. E.; Araki, K.; Eberlin, M. N. Protomers: formation, separation and characterization via travelling wave ion mobility mass spectrometry. *J. Mass Spectrom.* **2012**, *47* (6), 712−719.
(22) Kune, C.; Delvaux, C.; Haler, J. R. N.; Quinton, L.; Eppe, G.; De Pauw, E.; Far, J. A Mechanistic Study of Protonated Aniline to Protonated Phenol Substitution Considering Tautomerization by Ion Mobility Mass Spectrometry and Tandem Mass Spectrometry. *J. Am. Soc. Mass Spectrom.* **2019**, *30* (11), 2238−2249.
(23) Walker, S. W. C.; Mark, A.; Verbuyst, B.; Bogdanov, B.; Campbell, J. L.; Hopkins, W. S. Characterizing the Tautomers of Protonated Aniline Using Differential Mobility Spectrometry and Mass Spectrometry. *J. Phys. Chem. A* **2018**, *122* (15), 3858−3865.
(24) Attygalle, A. B.; Xia, H. X.; Pavlov, J. Influence of Ionization Source Conditions on the Gas-Phase Protomer Distribution of Anilinium and Related Cations. *J. Am. Soc. Mass Spectrom.* **2017**, *28* (8), 1575−1586.
(25) Xia, H.; Attygalle, A. B. Untrapping Kinetically Trapped Ions: The Role of Water Vapor and Ion-Source Activation Conditions on the Gas-Phase Protomer Ratio of Benzocaine Revealed by Ion-Mobility Mass Spectrometry. *J. Am. Soc. Mass Spectrom.* **2017**, *28* (12), 2580−2587.
(26) Patrick, A. L.; Cismesia, A. P.; Tesler, L. F.; Polfer, N. C. Effects of ESI conditions on kinetic trapping of the solution-phase protonation isomer of p-aminobenzoic acid in the gas phase. *Int. J. Mass Spectrom.* **2017**, *418*, 148−155.
(27) Seo, J.; Warnke, S.; Gewinner, S.; Schollkopf, W.; Bowers, M. T.; Pagel, K.; von Helden, G. The impact of environment and resonance effects on the site of protonation of aminobenzoic acid derivatives. *Phys. Chem. Chem. Phys.* **2016**, *18* (36), 25474−25482.
(28) Kumar, R.; Kenttämaa, H. I. Effects of Analyte Concentration on the Protonation Sites of 4-Aminobenzoic Acid upon Atmospheric Pressure Chemical Ionization As Revealed by Gas-Phase Ion−Molecule Reactions. *J. Am. Soc. Mass Spectrom.* **2020**, *31* (10), 2210−2217.
(29) Campbell, J. L.; Yang, A. M.-C.; Melo, L. R.; Hopkins, W. S. Studying Gas-Phase Interconversion of Tautomers Using Differential Mobility Spectrometry. *J. Am. Soc. Mass Spectrom.* **2016**, *27* (7), 1277−1284.
(30) Xia, H.; Attygalle, A. B. Effect of Electrospray Ionization Source Conditions on the Tautomer Distribution of Deprotonated p-Hydroxybenzoic Acid in the Gas Phase. *Anal. Chem.* **2016**, *88* (11), 6035−6043.
(31) Ohshimo, K.; Miyazaki, S.; Hattori, K.; Misaizu, F. Long-distance proton transfer induced by a single ammonia molecule: ion mobility mass spectrometry of protonated benzocaine reacted with NH3. *Phys. Chem. Chem. Phys.* **2020**, *22* (15), 8164−8170.
(32) Xia, H.; Attygalle, A. B. Transformation of the gas-phase favored O-protomer of p-aminobenzoic acid to its unfavored N-protomer by ion activation in the presence of water vapor: An ion-mobility mass spectrometry study. *J. Mass Spectrom.* **2018**, *53* (4), 353−360.
(33) Cismesia, A. P.; Nicholls, G. R.; Polfer, N. C. Amine vs. carboxylic acid protonation in ortho-, meta-, and para-aminobenzoic acid: An IRMPD spectroscopy study. *J. Mol. Spectrosc.* **2017**, *332*, 79−85.
(34) Boschmans, J.; Jacobs, S.; Williams, J. P.; Palmer, M.; Richardson, K.; Giles, K.; Lapthorn, C.; Herrebout, W. A.; Lemiere, F.; Sobott, F. Combining density functional theory (DFT) and collision cross-section (CCS) calculations to analyze the gas-phase behaviour of small molecules and their protonation site isomers. *Analyst* **2016**, *141* (13), 4044−4054.
(35) Marlton, S. J. P.; McKinnon, B. I.; Ucur, B.; Maccarone, A. T.; Donald, W. A.; Blanksby, S. J.; Trevitt, A. J. Selecting and identifying gas-phase protonation isomers of nicotineH(+) using combined laser, ion mobility and mass spectrometry techniques. *Faraday Discuss.* **2019**, *217*, 453−475.
(36) Matthews, E.; Dessent, C. E. Locating the Proton in Nicotinamide Protomers via Low-Resolution UV Action Spectroscopy of Electrosprayed Solutions. *J. Phys. Chem. A* **2016**, *120* (46), 9209−9216.
(37) Warnke, S.; Seo, J.; Boschmans, J.; Sobott, F.; Scrivens, J. H.; Bleiholder, C.; Bowers, M. T.; Gewinner, S.; Schollkopf, W.; Pagel, K.; von Helden, G. Protomers of benzocaine: solvent and permittivity dependence. *J. Am. Chem. Soc.* **2015**, *137* (12), 4236−4242.
(38) Ogorzalek Loo, R. R.; Lakshmanan, R.; Loo, J. A. What Protein Charging (and Supercharging) Reveal about the Mechanism of Electrospray Ionization. *J. Am. Soc. Mass Spectrom.* **2014**, *25* (10), 1675−1693.
(39) Zenaidee, M. A.; Leeming, M. G.; Zhang, F.; Funston, T. T.; Donald, W. A. Highly Charged Protein Ions: The Strongest Organic Acids to Date. *Angew. Chem., Int. Ed.* **2017**, *56* (29), 8522−8526.
(40) Going, C. C.; Williams, E. R. Supercharging with m-nitrobenzyl alcohol and propylene carbonate: forming highly charged ions with extended, near-linear conformations. *Anal. Chem.* **2015**, *87* (7), 3973−3980.
(41) Shimizu, L. S.; Smith, M. D.; Hughes, A. D.; Shimizu, K. D. Self-assembly of a bis-urea macrocycle into a columnar nanotube. *Chem. Commun.* **2001**, *17*, 1592−1593.
(42) Sindt, A. J.; Smith, M. D.; Pellechia, P. J.; Shimizu, L. S. Thioureas and Squaramides: Comparison with Ureas as Assembly Directing Motifs for m-Xylene Macrocycles. *Cryst. Growth Des.* **2018**, *18* (3), 1605−1612.
(43) Som, B.; Salpage, S. R.; Son, J.; Gu, B.; Karakalos, S. G.; Smith, M. D.; Shimizu, L. S. Pillars of assembled pyridyl bis-urea macrocycles: a robust synthon to organize diiodotetrafluorobenzenes. *CrystEngComm* **2017**, *19* (3), 484−491.
(44) Roy, K.; Wang, C.; Smith, M. D.; Dewal, M. B.; Wibowo, A. C.; Brown, J. C.; Ma, S.; Shimizu, L. S. Guest induced transformations of assembled pyridyl bis-urea macrocycles. *Chem. Commun.* **2011**, *47* (1), 277−9.
(45) Gabelica, V.; Livet, S.; Rosu, F. Optimizing Native Ion Mobility Q-TOF in Helium and Nitrogen for Very Fragile Noncovalent Structures. *J. Am. Soc. Mass Spectrom.* **2018**, *29* (11), 2189−2198.
(46) Hawkins, P. C. D.; Skillman, A. G.; Warren, G. L.; Ellingson, B. A.; Stahl, M. T. Conformer Generation with OMEGA: Algorithm and Validation Using High Quality Structures from the Protein Databank and Cambridge Structural Database. *J. Chem. Inf. Model.* **2010**, *50* (4), 572−584.
(47) Shvartsburg, A. A.; Jarrold, M. F. An exact hard-spheres scattering model for the mobilities of polyatomic ions. *Chem. Phys. Lett.* **1996**, *261*, 86−91.
(48) Mesleh, M. F.; Hunter, J. M.; Shvartsburg, A. A.; Schatz, G. C.; Jarrold, M. F. Structural Information from Ion Mobility Measurements: Effects of the Long-Range Potential. *J. Phys. Chem.* **1996**, *100*, 16082−16086.
(49) Hanwell, M. D.; Curtis, D. E.; Lonie, D. C.; Vandermeersch, T.; Zurek, E.; Hutchison, G. R. Avogadro: an advanced semantic chemical editor, visualization, and analysis platform. *J. Cheminform.* **2012**, *4* (1), 17.

https://doi.org/10.1021/jasms.2c00033
J. Am. Soc. Mass Spectrom. 2022, 33, 840−850

(50) Frisch, M. J.; Trucks, G. W.; Schlegel, H. B.; Scuseria, G. E.; Robb, M. A.; Cheeseman, J. R.; Scalmani, G.; Barone, V.; Petersson, G. A.; Nakatsuji, H.; Li, X.; Caricato, M.; Marenich, A. V.; Bloino, J.; Janesko, B. G.; Gomperts, R.; Mennucci, B.; Hratchian, H. P.; Ortiz, J. V.; Izmaylov, A. F.; Sonnenberg, J. L.; Williams-Young, D.; Ding, F.; Lipparini, F.; Egidi, F.; Goings, J.; Peng, B.; Petrone, A.; Henderson, T.; Ranasinghe, D.; Zakrzewski, V. G.; Gao, J.; Rega, N.; Zheng, G.; Liang, W.; Hada, M.; Ehara, M.; Toyota, K.; Fukuda, R.; Hasegawa, J.; Ishida, M.; Nakajima, T.; Honda, Y.; Kitao, O.; Nakai, H.; Vreven, T.; Throssell, K.; Montgomery, J. A., Jr.; Peralta, J. E.; Ogliaro, F.; Bearpark, M. J.; Heyd, J. J.; Brothers, E. N.; Kudin, K. N.; Staroverov, V. N.; Keith, T. A.; Kobayashi, R.; Normand, J.; Raghavachari, K.; Rendell, A. P.; Burant, J. C.; Iyengar, S. S.; Tomasi, J.; Cossi, M.; Millam, J. M.; Klene, M.; Adamo, C.; Cammi, R.; Ochterski, J. W.; Martin, R. L.; Morokuma, K.; Farkas, O.; Foresman, J. B.; Fox, D. J. *Gaussian 16*, revision B.01; Gaussian, Inc.: Wallingford, CT, 2016.
(51) Becke, A. D. Density-functional thermochemistry. III. The role of exact exchange. *J. Chem. Phys.* **1993**, *98*, 5648−5652.
(52) Lee, C.; Yang, W.; Parr, R. G. Development of the Colle-Salvetti correlation-energy formula into a functional of the electron density. *Phys. Rev. B* **1988**, *37*, 785−789.
(53) Vosko, S. H.; Wilk, L.; Nusair, M. Accurate spin-dependent electron liquid correlation energies for local spin density calculations: a critical analysis. *Can. J. Phys.* **1980**, *58*, 1200−1211.
(54) Stephens, P. J.; Devlin, F. J.; Chabalowski, C. F.; Frisch, M. J. Ab Initio Calculation of Vibrational Absorption and Circular Dichroism Spectra Using Density Functional Force Fields. *J. Phys. Chem.* **1994**, *98* (45), 11623−11627.
(55) Hellweg, A.; Rappoport, D. Development of new auxiliary basis functions of the Karlsruhe segmented contracted basis sets including diffuse basis functions (def2-SVPD, def2-TZVPPD, and def2-QVPPD) for RI-MP2 and RI-CC calculations. *Phys. Chem. Chem. Phys.* **2015**, *17*, 1010−1017.
(56) Grimme, S.; Antony, J.; Ehrlich, S.; Krieg, H. A consistent and accurate ab initio parameterization of density functional dispersion correction (DFT-D) for the 94 elements H-Pu. *J. Chem. Phys.* **2010**, *132*, 154104.
(57) Qin, L.; Hartley, A.; Turner, P.; Elmes, R. B. P.; Jolliffe, K. A. Macrocyclic squaramides: anion receptors with high sulfate binding affinity and selectivity in aqueous media. *Chem. Sci.* **2016**, *7* (7), 4563−4572.
(58) Qin, L.; Wright, J. R.; Lane, J. D. E.; Berry, S. N.; Elmes, R. B. P.; Jolliffe, K. A. Receptors for sulfate that function across a wide pH range in mixed aqueous-DMSO media. *Chem. Commun.* **2019**, *55*, 12312.
(59) Shrivastav, V.; Nahin, M.; Hogan, C. J.; Larriba-Andaluz, C. Benchmark Comparison for a Multi-Processing Ion Mobility Calculator in the Free Molecular Regime. *J. Am. Soc. Mass Spectrom.* **2017**, *28* (8), 1540−1551.
(60) Zhang, L.; Wang, Y.; Zheng, F.; Zhu, D.; Liang, Y.; Shi, Q. Influence Exerted by the Solvent Effect on the Mobility Peak of 1,8-Naphthalic Anhydride in Ion Mobility Spectrometry. *J. Am. Soc. Mass Spectrom.* **2022**, *33* (3), 457−462.
(61) Kurulugama, R. T.; Darland, E.; Kuhlmann, F.; Stafford, G.; Fjeldsted, J. Evaluation of drift gas selection in complex sample analyses using a high performance drift tube ion mobility-QTOF mass spectrometer. *Analyst* **2015**, *140* (20), 6834−6844.
(62) Morris, C. B.; May, J. C.; Leaptrot, K. L.; McLean, J. A. Evaluating Separation Selectivity and Collision Cross Section Measurement Reproducibility in Helium, Nitrogen, Argon, and Carbon Dioxide Drift Gases for Drift Tube Ion Mobility-Mass Spectrometry. *J. Am. Soc. Mass Spectrom.* **2019**, *30* (6), 1059−1068.
(63) Asbury, G. R.; Hill, H. H. Using Different Drift Gases To Change Separation Factors (α) in Ion Mobility Spectrometry. *Anal. Chem.* **2000**, *72*, 580−584.
(64) West, R. C.; Lide, D. R. *CRC Handbook of Chemistry and Physics*, 70th ed.; CRC Press: Boca Raton, FL, 1989.
(65) Gray, A. L. H.; Antevska, A.; Oluwatoba, D. S.; Schonfeld, G. E.; Lazar Cantrell, K. L.; Do, T. D. Cytotoxicity of alpha-Helical, Staphylococcus aureus PSMalpha3 Investigated by Post-Ion-Mobility Dissociation Mass Spectrometry. *Anal. Chem.* **2020**, *92* (17), 11802−11808.
(66) Zheng, Z.; Attygalle, A. B. Impact of Ambient Vapors Present in an Electrospray Ionization Source on Gas-Phase Ion Structures. *J. Am. Soc. Mass Spectrom.* **2021**, *32* (3), 725−735.
(67) Groenenboom, M. C.; Saravanan, K.; Zhu, Y.; Carr, J. M.; Marjolin, A.; Faura, G. G.; Yu, E. C.; Dominey, R. N.; Keith, J. A. Structural and Substituent Group Effects on Multielectron Standard Reduction Potentials of Aromatic N-Heterocycles. *J. Phys. Chem. A* **2016**, *120* (34), 6888−94.
(68) Schrage, B. R.; Nemykin, V. N.; Ziegler, C. J. Biliazine: a ring open phthalocyanine analog with a meso hydrogen bond. *Chem. Commun.* **2020**, *56* (49), 6628−6631.
(69) Schiessl, W. C.; Summa, N. K.; Weber, C. F.; Gubo, S.; Ducker-Benfer, C.; Puchta, R.; van Eikema Hommes, N. J. R.; van Eldik, R. Experimental and Theoretical Approaches to the Protonation of Thiourea: A Convenient Nucleophile in Coordination Chemistry Revisited. *Z. Anorg. Allg. Chem.* **2005**, *631*, 2812−2819.
(70) Janssen, M. J. The structure of protonated amides and ureas and their thio analogues. *Spectrochim. Acta* **1961**, *17*, 475−485.
(71) Wen, N. P.; Brooker, M. H. Urea Protonation - Raman and Theoretical-Study. *J. Phys. Chem.* **1993**, *97* (33), 8608−8616.

https://doi.org/10.1021/jasms.2c00033
J. Am. Soc. Mass Spectrom. 2022, 33, 840−850